

ARTICLE TYPE

One machine, one minute, three billion tetrahedra

Célestin Marot* | Jeanne Pellerin | Jean-François Remacle

¹Université catholique de Louvain, iMMC,
Avenue Georges Lemaitre 4, bte L4.05.02,
1348 Louvain-la-Neuve, Belgium

Correspondence

*Corresponding author: Email:
celestin.marot@uclouvain.be

Summary

This paper presents a new scalable parallelization scheme to generate the 3D Delaunay triangulation of a given set of points. Our first contribution is an efficient serial implementation of the incremental Delaunay insertion algorithm. A simple dedicated data structure and a number of improvements in the insertion algorithm have permitted to accelerate by a factor three reference implementations. Our second contribution is a multi-threaded version of the Delaunay kernel able to concurrently insert vertices. Moore curve coordinates are used to partition the point set, avoiding so heavy synchronization overheads. Conflicts are managed by modification of the partition with a simple rescaling of the space-filling curve. The performances of our implementation have been measured on three different processors, Intel core-i7, Intel Xeon Phi and AMD EPYC, on which we have been able to compute 3 billion tetrahedra in 53 seconds. This corresponds to a generation rate of over 55 million tetrahedra per second which is, to our best knowledge, three times the rate reached by the current fastest implementation. It is finally shown how this very efficient parallel Delaunay triangulation can be integrated in a Delaunay refinement mesh generator taking as input the boundary of the domain to mesh.

KEYWORDS:

Tetrahedral mesh generation; parallel Delaunay triangulation; Delaunay refinement; Hilbert curve; SFC partitioning

1 | INTRODUCTION

Delaunay refinement is a technique to generate triangular or tetrahedral unstructured meshes suitable for finite element analysis. The principle of Delaunay refinement-based mesh generators is to refine an initially coarse boundary conforming mesh by inserting successively vertices that improve the mesh quality, but holding the Delaunay geometrical condition verified all the time. Delaunay refinement-based mesh generators have been used since the 1980's in the engineering community, and are the kernel of most industrial-grade mesh generators. This is due to two key advantages over concurrent techniques:

- **Robustness:** They maintain a valid mesh throughout, ensuring that a usable mesh is always produced even when the refinement process would fail. This is a striking advantage over frontal approaches.
- **Speed:** They are fast because, in practice, a vertex can be inserted in constant time.

State-of-the art 3D mesh generation algorithms generate about 5 million tetrahedra per minute on one single core¹, including I/O operations.

¹<http://www.meshgems.com/white-papers.php>

The most computationally expensive step in such Delaunay based mesher is the construction of the Delaunay triangulation of a given set of points. The main ingredients for fast Delaunay triangulations are known (see the book of Cheng et al.¹ for a comprehensive and exhaustive review). Tetgen², CGAL³ and Geogram⁴ are the most efficient open-source programs at computing Delaunay triangulations. They are designed similarly and offer similar performances, i.e., they triangulate 10^6 points in about 6 seconds on one core of a high-end laptop. Such performances may seem sufficient for most applications, but the size of industrial meshes has considerably grown in the last decades, due to the increased availability of massively parallel numerical solvers. It is now common to deal with meshes of over several hundred millions of tetrahedra. Moreover, the construction of a computational mesh often requires in practice the generation of several intermediate meshes, iteratively enhanced to fulfill specific design requirements. The mesh generation process is therefore nowadays considered a technological bottleneck in computational engineering⁵.

To overcome these limitations, parallel mesh generation procedures have been proposed for the last two decades⁶. Most of them rely on a domain decomposition strategy and apply to each sub-domain an “off the shelf” meshing algorithm^{7,8}. The difficulty is then to ensure mesh compatibility across sub-domain boundaries. This kind of parallelization, called coarse grain domain decomposition, has allowed building significantly larger meshes with existing serial meshing algorithms, but no significant acceleration of the meshing algorithm itself is involved. The overheads are rather high, and the scaling pretty bad.

A much better approach is to work at a fine grain level, and to perform point insertion and local mesh modification in a concurrent fashion. Delaunay-based algorithms relies indeed on few “fine grain” operations, which only affect a small number of elements: point insertion, edge swap, vertex relocation, point deletion. The challenge in parallelizing these operations is to appropriately manage conflicts, as two threads cannot modify the same tetrahedron. On relatively small number of cores, interesting speedups of 5 on 8 cores and 18 on 32 cores have been obtained by Batista⁹ and Remacle¹⁰. But synchronization overheads prevent these methods to scale for larger number of cores.

In this paper we propose a scalable parallel Delaunay refinement meshing algorithm focusing first on the core of unstructured tetrahedral meshing, i.e., the construction of the Delaunay triangulation of a given set of points. Our first contribution is a sequential implementation of the Delaunay triangulation algorithm that is able to triangulate a million points in about 2 seconds, which is three times faster than reference implementations. The implementation is based on the state-of-the-art incremental Delaunay insertion algorithm^{2,3,4}, but the gain in performance is to ascribe to the details of the specific data structures we have developed, to the optimization of geometric predicates evaluation, and to specialized adjacency computations (§2).

Our second contribution is a scalable multicore version of the Delaunay triangulation algorithm in 3D devoid of heavy synchronization overheads (§3). The domain is partitioned using Hilbert coordinates and conflicts are detected with a simple coloring scheme. The performances and scalability have been demonstrated on three different machines: a high-end four core laptop, a 64 core Intel[®] Xeon Phi Knight’s Landing, and a recent AMD[®] EPYC 64 core machine (§3.7). On the latter computer, we have been able to generate three billion tetrahedra in less than a minute (about 10^7 points per second).

We finally demonstrate how the efficient Delaunay triangulation can be easily integrated in a tetrahedral mesh generation process where the input is the boundary of a domain to mesh (§4).

2 | SEQUENTIAL DELAUNAY

The Delaunay triangulation $DT(S)$ of a point set S has the fundamental geometrical property that the circumsphere of any tetrahedron contains no other point of S than those of the considered tetrahedron. This property is of particular interest for mesh generation since, in contrast to many other triangulations, a Delaunay triangulation produces tetrahedra suitable for numerical methods.

More formally, a triangulation³ $T(S)$ of the n points $S = \{p_1, \dots, p_n\} \in \mathbb{R}^3$ is a set of non overlapping tetrahedra that covers exactly the convex hull $\Omega(S)$ of the point set, and leaves no point p_i isolated. If the empty circumsphere condition is verified for all tetrahedra, the triangulation $T(S)$ is said to be a Delaunay triangulation. If additionally S contains no group of 4 coplanar points and no group of 5 cospherical points, then it is said to be in general position, and the Delaunay triangulation $DT(S)$ is then unique.

Delaunay-based mesh generators incrementally insert points in an initial Delaunay triangulation, and ingredients for fast serial algorithms with $\mathcal{O}(n \log n)$ complexity are known and have been documented¹. Efficient open-source implementations

²<https://project.inria.fr/pampa/>

³This paper is about 3D meshing. Still we use the generic term triangulation instead of tetrahedralization

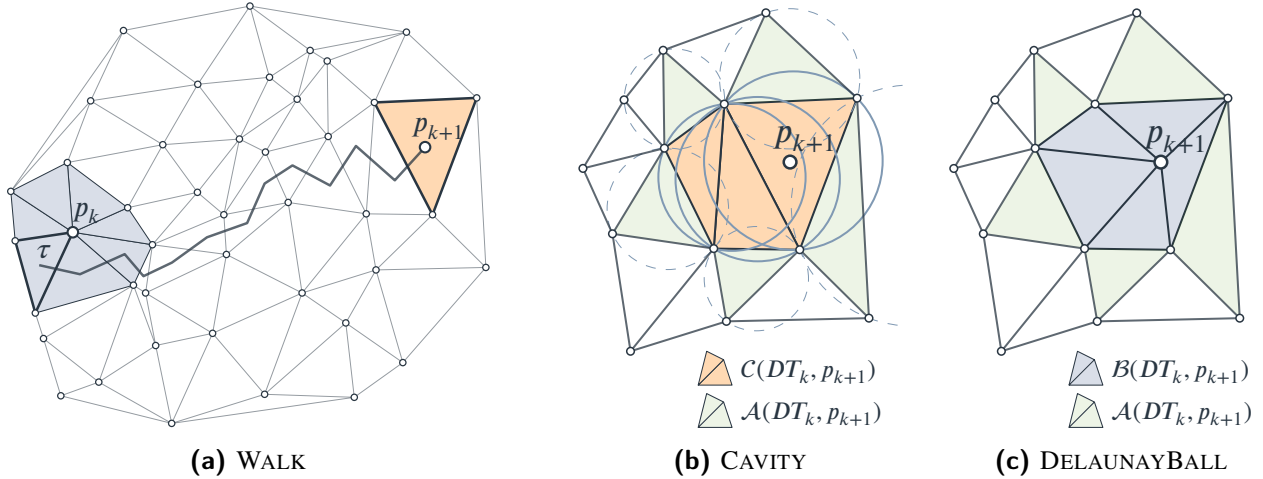


FIGURE 1 Insertion of a vertex p_{k+1} in the Delaunay triangulation DT_k . The triangle containing p_{k+1} is obtained by walking toward p_{k+1} . The WALK (a) starts from $\tau \in \mathcal{B}_{p_k}$. The CAVITY function (b) finds all cavity triangles (orange). These are the triangles whose circumsphere contains the vertex p_{k+1} . Cavity triangles are deleted, while cavity adjacent triangles (green) are kept. The DELAUNAYBALL function (c) creates new triangles (blue) by connecting p_{k+1} to the edges of the cavity boundary.

are available: Tetgen², CGAL³ and Geogram⁴. They are designed similarly and offer therefore similar performances (Table 1). In the following, the incremental insertion algorithm is recalled, before giving more details on the dedicated data structures we have developed and the algorithmic optimizations that make our implementation three times faster.

2.1 | Overview of performance improvements

The fastest algorithm to build the 3D Delaunay triangulation, $DT(S)$, works by incremental insertion of points in the triangulation. The algorithm has a $\mathcal{O}(n \log n)$ complexity¹¹, and is presented in (§2.1).

Let DT_k be the Delaunay triangulation of the subset $S_k = \{p_1, \dots, p_k\} \subset S$. The *Delaunay kernel* is the procedure to insert a new point $p_{k+1} \in \Omega(S_k)$ into DT_k , and construct a new valid Delaunay triangulation DT_{k+1} of $S_{k+1} = \{p_1, \dots, p_k, p_{k+1}\}$. The *Delaunay kernel* can be written in the following abstract manner:

$$DT_{k+1} \leftarrow DT_k - C(DT_k, p_{k+1}) + B(DT_k, p_{k+1}), \quad (1)$$

where the Delaunay cavity $C(DT_k, p_{k+1})$ is the set of all tetrahedra whose circumsphere contains p_{k+1} (Figure 1b), whereas the Delaunay ball $B(DT_k, p_{k+1})$ is a set of tetrahedra filling up the polyhedral hole obtained by removing the Delaunay cavity $C(DT_k, p_{k+1})$ from DT_k (Figure 1c).

We have implemented the state-of-the-art algorithm (Algorithm 1). The open-source code has about one thousand lines and is available in HXT (www.hextreme.eu). The important steps of the algorithm are as follows.

INIT

The triangulation is initialized with the tetrahedron formed by the first four non-coplanar vertices of the point set S . They define a tetrahedron τ with a positive volume.

SORT

Sorting points is the algorithm bottleneck for very large point sets². So we have implemented a very fast sorting procedure (Section 2.3). Points are sorted in such a way that two points that are close in space have close indices. This ordering has for consequence that the cavities $C(DT_k, p_{k+1})$ contain less tetrahedra. After appropriate sorting, the kernel functions WALK, CAVITY and DELAUNAYBALL have constant complexity. The sorting step is thus crucial for the algorithm efficiency.

WALK

The goal of this step is to identify the tetrahedron τ_{k+1} enclosing the next point to insert p_{k+1} . The search starts from the tetrahedron τ_k containing the last inserted point p_k , and walks through the current triangulation DT_k in direction of p_{k+1} (Figure 1a).

We say that a point is visible from a facet when the tetrahedron defined by this facet and this point has negative volume. The WALK function thus iterates on the four facets of τ , selects one from which the point p_{k+1} is visible, and walk then across this facet to the adjacent tetrahedron. This new tetrahedron is called τ and the WALK process is repeated until none of the facets of τ sees p_{k+1} , which is equivalent to say that p_{k+1} is inside τ (see Figure 1a).

The visibility walk algorithm is guaranteed to terminate for Delaunay triangulations¹². If the points have been sorted as described above, the number of walking steps is essentially constant¹⁰. Our implementation of this robust and efficient walking algorithm is similar to other available implementations.

CAVITY

Once the tetrahedron $\tau \leftarrow \tau_{k+1}$ that contains the point to insert p_{k+1} has been identified, the function CAVITY finds all tetrahedra whose circumsphere contain p_{k+1} and delete them. The Delaunay cavity $\mathcal{C}(\text{DT}_k, p_{k+1})$ is simply connected and contains τ ¹³, it is then built using a breadth-first search algorithm. The core and most expensive operation of the CAVITY function is the `inSphere` predicate, which evaluates whether a point e is inside/on or outside the circumsphere of given tetrahedron. This CAVITY function is thus an expensive function of the incremental insertion, which accounts for about 33% of the total computation time (Table 1). To accelerate this, we propose in Section 2.4 to precompute sub-components of the `inSphere` predicate.

DELAUNAYBALL

Once the cavity has been carved, the DELAUNAYBALL function generates first a set of new tetrahedra adjacent to the newly insert point p_{k+1} and filling up the cavity, and updates then the mesh structure. Mesh update consists in particular in the computation of adjacencies between the newly created tetrahedra. This is the most expensive step of the algorithm, with about 39% of the total computation time (Table 1). To accelerate this step, we replace general purpose elementary operations like tetrahedron creation/deletion or adjacency computation, with batches of optimized operations making benefit from a cavity-specific data structure (Section 2.5).

Algorithm 1 Sequential computation of the Delaunay Triangulation DT of a set of vertices S

Input: S

Output: $\text{DT}(S)$

▷ Section 2.2

```

1: function SEQUENTIAL_DELAUNAY( $S$ )
2:    $\tau \leftarrow \text{INIT}(S)$ 
3:    $\text{DT} \leftarrow \tau$ 
4:    $S' \leftarrow S \setminus \tau$ 
5:    $S' \leftarrow \text{SORT}(S')$                                      ▷ Section 2.3
6:   for all  $p \in S'$  do
7:      $\tau \leftarrow \text{WALK}(\text{DT}, \tau, p)$ 
8:      $\mathcal{C} \leftarrow \text{CAVITY}(\text{DT}, \tau, p)$                        ▷ Section 2.4
9:      $\text{DT} \leftarrow \text{DT} \setminus \mathcal{C}$ 
10:     $\mathcal{B} \leftarrow \text{DELAUNAYBALL}(\mathcal{C}, p)$                        ▷ Section 2.5
11:     $\text{DT} \leftarrow \text{DT} \cup \mathcal{B}$ 
12:     $\tau \leftarrow t \in \mathcal{B}$ 
13:  end for
14:  return  $\text{DT}$ 
15: end function

```

2.2 | Mesh data structure

One key for enhancing performances of a Delaunay triangulation algorithm resides in the optimization of the data structure used to store the mesh. Various data structure designs have been proposed that are very flexible and allow representing hybrid meshes, high order meshes, add mesh elements of any type, or manage adjacencies around vertices, edges, etc. The versatility of such general purpose data structures has a cost, both in terms of storage and efficiency. Here, our aim is to have a structure

	Ours	Geogram	TetGen
SEQUENTIAL_DELAUNAY	12.7	34.6	32.9
INIT + SORT	0.5	4.2	2.1
INCREMENTAL INSERTION	12.2	30.4	30.8
WALK	1.0	2.1	1.6
orient3d	0.7	1.4	1.1
CAVITY	6.2	11.4	≈ 10
inSphere	3.2	6.2	5.6
DELAUNAYBALL	4.5	12.4	≈ 15
Computing sub-determinants	1.3	/	/
Other operations	0.5	4.5	≈ 4

TABLE 1 Timings for the different steps of the Delaunay incremental insertion algorithm (Algorithm 1) for three implementations: ours, Geogram⁴, and Tetgen². Timings in seconds are given for 5 million vertices (random uniform distribution). The ≈ prefix indicates that no accurate timing is available.

```

5 typedef struct {
    double coordinates[3];
    uint64_t padding;
} point3d_t;

10 typedef struct {
    struct {
        uint32_t* vertex_ID;
        uint64_t* neighbor_ID;
        double* sub_determinant;
        uint64_t num;
        uint64_t allocated_num; // number of tetrahedra
        uint64_t capacity; // capacity [in tetrahedra]
    } tetrahedra;

15     struct {
        point3d_t* vertex;
        uint32_t num;
        uint32_t allocated_num; // number of vertices
        uint32_t capacity; // capacity [in vertices]
    } vertices;

20 } mesh_t;

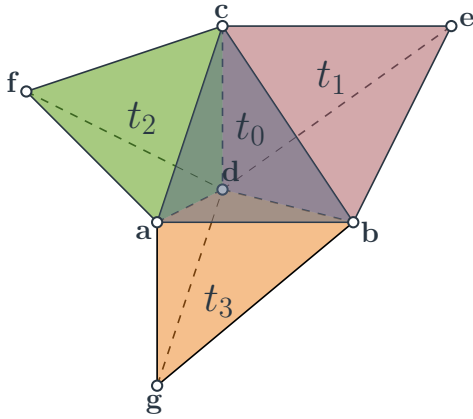
```

Listing 1: The aligned mesh data structure `mesh_t` we use to store the vertices and tetrahedra of a Delaunay triangulation in 3D

as lightweight and fast as possible, dealing exclusively with 3D meshing. Our implementation is coded in plain C language, with arrays of doubles, floats, and integers to store mesh topology and geometry. This seemingly old-style coding has important advantages in terms of optimization and parallelization because it compels to use simple and straightforward algorithms. Moreover, it allows fine grain memory optimizations, like data alignment and cache miss rate reduction.

The mesh data only contains vertices and tetrahedra explicitly, and all topological and geometrical information can be deduced from it. However, in order to speed up mesh operations, it is beneficial to store additional connectivity information. A careful trade-off needs however to be made between computational time and memory space. The only connectivity information we have chosen to store is the adjacency between tetrahedra, as this allows walking through the mesh using local queries only.

Vertices Vertices are stored in a single array of structures `point3d_t` (see Listing 1). For each vertex, in addition to the vertex coordinates, a padding variable is used to align the structure to 32 bytes (3 doubles of 8 bytes each, and an additional padding variable of 8 bytes sum up to a structure of 32 bytes) and conveniently store temporarily some auxiliary vertex related values at different stages of the algorithms. Memory alignment ensures that a vertex would not overlap two cache lines during memory transfer. Modern computers usually work with cache lines of 64 bytes. With the padding variable in the vertex structure, a vertex is guaranteed to always be loaded in one single memory fetch. Moreover, aligned memory is necessary for taking advantage of the vectorization capabilities of modern microprocessors.



memory index	vertex_ID	neighbor_ID
$4t_0$	a	$4t_1 + 3$
$4t_0 + 1$	b	$4t_2 + 3$
$4t_0 + 2$	c	$4t_3 + 3$
$4t_0 + 3$	d	—
:		
$4t_1$	b	—
$4t_1 + 1$	c	—
$4t_1 + 2$	d	—
$4t_1 + 3$	e	$4t_0 + 0$
:		
$4t_2$	a	—
$4t_2 + 1$	d	—
$4t_2 + 2$	c	—
$4t_2 + 3$	f	$4t_0 + 1$
:		
$4t_3$	a	—
$4t_3 + 1$	b	—
$4t_3 + 2$	d	—
$4t_3 + 3$	g	$4t_0 + 2$

FIGURE 2 Four adjacent tetrahedra : t_0, t_1, t_2, t_3 and one of their possible memory representation in the tetrahedra data structure given in Listing 1. `tetrahedra_neighbor_ID[$4t_i + j$]/4` gives the index of adjacent tetrahedra opposite to `tetrahedra_vertex_ID[$4t_i + j$]` in tetrahedra t_i and `tetrahedra_neighbor_ID[$4t_i + j$]` gives the index where the inverse adjacency is stored.

Tetrahedra Each tetrahedron knows about its 4 vertices and its 4 neighboring tetrahedra. These two kinds of adjacency data are however stored in two separate arrays, and not tetrahedron by tetrahedron. The main motivation for that is flexibility and again memory alignment. Keeping good memory alignment properties on a tetrahedron structure evolving with the implementation is cumbersome. In addition, it provides little to no performance gain in this case. On the other hand with parallel arrays, additional information per tetrahedron (e.g. a color for each tetrahedron, sub-determinants...) can be added easily without disrupting the whole memory layout. For this reason, element vertices and element neighbors are stored in two separate arrays. Each tetrahedron is identified by the indices of its four vertices in the `vertices` structure. Vertex indices of tetrahedron t are read between positions $4*t$ and $4*t+3$ in the global array `tetrahedra_vertex_ID` storing all tetrahedron vertices. Vertex are ordered so that the volume of the tetrahedron is positive. An array of double, `sub_determinant`, is used to store 4 values per tetrahedron. This space is used to speed up geometric predicate evaluation (see Section 2.4).

Adjacencies By convention, the i -th facet of a tetrahedron is the facet opposite the i -th vertex, and the i -th neighbor is the tetrahedron adjacent to that facet. In order to travel efficiently through the mesh, facet indices are stored together with the indices of the corresponding adjacent tetrahedron, thanks to an integer division and its modulo. The scheme is simple. Each adjacency is represented by the integer obtained by multiplying by four the index of the tetrahedron and adding the internal index of the facet in the tetrahedron. Take, for instance, two tetrahedra t_1 and t_2 sharing facet f , whose indice is respectively i_1 in t_1 and i_2 in t_2 . The adjacency is then represented as `tetrahedra_neighbor_ID[$4t_1+i_1$]`= $4t_2+i_2$ and `tetrahedra_neighbor_ID[$4t_2+i_2$]`= $4t_1+i_1$. This multiplexing avoids a costly looping over the facets of a tetrahedron. The fact that it reduces by a factor 4 the maximum number of tetrahedron in a mesh is not a real concern since, element indices being stored as 64 bytes unsigned integers, the maximal number of element in a mesh is `UINT64_MAX`= $2^{64} \simeq 1.8 \cdot 10^{19}$, which is huge. Note also that division by 4 is a very cheap bitwise left-shift operation for an unsigned integers i , i.e., $i/4 = i \gg 2$.

Memory footprint The key to an efficient data structure is the the balance between its memory footprint and its efficiency. We do not expect to generate meshes of more than `UINT32_MAX` vertices, i.e. about 4 billion vertices on one single machine. Each vertex therefore occupies 32 bytes, 24 bytes for its coordinates and 8 bytes for the padding variable. On the other hand, the number of tetrahedra could itself be larger than 4 billion, so that a 64 bits integer is needed for element indexing. Each tetrahedron occupies 80 bytes, $4 \times 4 = 16$ bytes for the vertices, $4 \times 8 = 32$ bytes for the neighbors, 32 bytes again for the sub-determinants. In average a tetrahedral mesh of n vertices has a little more than $6n$ tetrahedra. Thus, our mesh data structure requires $\simeq 6 \times 80 + 32 = 512$ bytes per vertex.

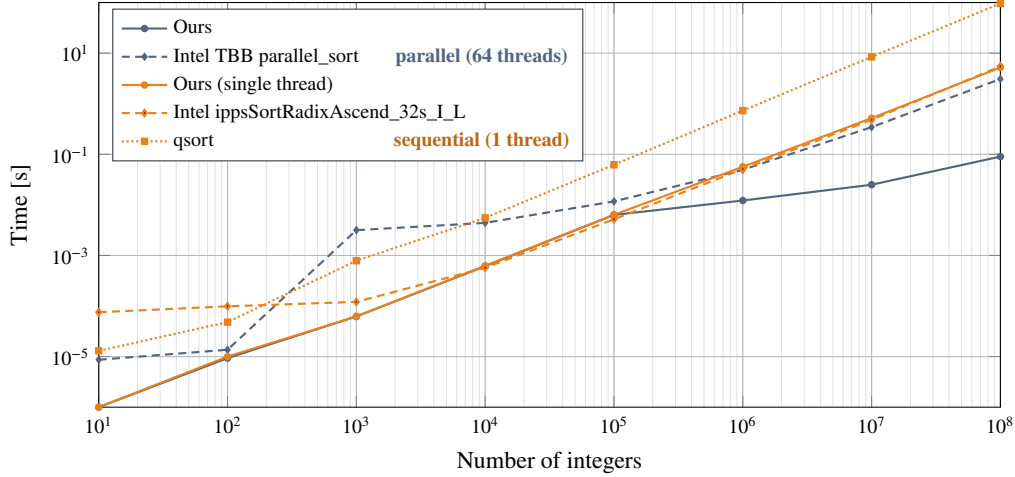


FIGURE 3 Performances of HXTSort for sorting 31-bit integers produced by `rand()` on an Intel® Xeon Phi™ 7210 CPU and comparison with widely used implementations. Each integer is both the key and the value.

2.3 | Fast spatial sorting

The complexity of the Delaunay triangulation algorithm depends on the number of tetrahedra traversed during the walking steps, and on the number of tetrahedra in the cavities. An appropriate spatial sorting is required to improve locality, i.e., reduce the walking steps, while retaining enough randomness to have cavity sizes independent of the number of vertices already inserted in the mesh (by cavity size, we mean the number of tetrahedra in the cavity, not the volume of the cavity).

An efficient spatial sorting scheme has been proposed by Boissonnat et al.¹⁴ and is used in state-of-the-art Delaunay triangulation implementations. The main idea is to first shuffle the vertices, and to group them in rounds of increasing size (a first round with, e.g., the first 1000 vertices, a second with the next 7000 vertices, etc.) as described by the Biased Randomized Insertion Order (BRIO)¹⁵. Then, each group is ordered following a space-filling curve. The space-filling curve should have the good locality properties that successive points on the curve are geometrically close to each other. With this spatial sorting, the number of walking steps between two successive cavities remains small and essentially constant¹⁰. On the other hand, proceeding by successive rounds according to the BRIO algorithm tends to reduce the average size of cavities.

The Hilbert curve is a continuous self-similar (fractal) curve. It has the interesting property to be space-filling, i.e., to visit exactly once all the cells of a regular grid with $2^m \times 2^m \times 2^m$ cells, $m \in \mathbb{N}$. A Moore curve is a closed Hilbert curve. Hilbert and Moore curves have the sought spatial locality properties, in the sense that points close to each other on the curve are also close to each other in \mathbb{R}^3 ^{16,17}. Any 3D point set can be ordered by a Hilbert/Moore curve according to the order in which the curve visits the grid cells that contains the points. The Hilbert/Moore index is thus an integer value $d \in \{0, 1, 2, \dots, 2^{3m} - 1\}$, and several points might have the same index. The bigger m is for a given point set, the smaller the grid cells are, and hence the lower the probability of having two points with the same Hilbert/Moore index. Given a 3D point set with n points, there are $n/2^{3m}$ points per grid cell in average, and choosing $m = k \log_2(n)$, with k a constant, ensures the average number of points in grid cells to be independent of n . For Delaunay triangulation purposes, the objective is both to limit the number of points with the same indices (in the same grid cell) and to have indices within the smallest range as possible to accelerate subsequent sorting operations. There is thus a balance to find, so that Hilbert indices are neither too dense nor too sparse.

Computing the Hilbert/Moore index of one cell is a somewhat technical point. The Hilbert/Moore curve is indeed fractal, which means recursively composed of replicas of itself that have been scaled down by a factor two, rotated and optionally reflected. Those reflections and rotations can be efficiently computed with bitwise operations. Various transformations can be applied to point coordinates to emulate non-regular grids, a useful functionality we will resort to in Section 3.3. Hamilton gives extensive details on how to compute Hilbert indices¹⁸.

Once the Hilbert/Moore indices have been computed, points can be sorted accordingly in a data structure where the Hilbert/Moore indice is the key, and the point the associated value. An extremely well suited strategy to sort bounded integer keys is the radix sort^{19,20,21,22}, a non-comparative sorting algorithm working digit by digit. The base of the digits, the radix, can be freely chosen.

Radix sort has a $O(wn)$ complexity, where n is the number of $\{key, value\}$ pairs and w the number of digits (or bits) of the keys. In our case, the radix sort has a complexity in $O(mn) = O(n \log_2(n))$, where n is the number of points and $m = k \log_2(n)$ the number of levels of the Hilbert/Moore grid. In general, m is small because a good resolution of the space-filling curve is not needed. Typically, the number of keys is lower than the number of values to be sorted. We say that keys are *short*. Radix-sort is able to sort such keys incredibly quickly which is why it is the only sorting algorithm to consider in this case.

Spatial sorting is the only part of the tetrahedrization process with a superlinear complexity. Making it really fast is thus crucial to our aim of building a fast mesh generator. Literature is abundant on parallel radix sorting and impressive performances are obtained on many-core CPUs and GPUs^{23,24,25,26,27,28}. However, implementations are seldom available and we were not able to find a parallel radix sort implementation properly designed for many-core CPUs. Therefore, we made an own implementation, called `HXTSort`, and available as open source at <https://www.hextreme.eu/hxtsort>. It is easy to use and comes with proper documentation. Figure 3 compares `HXTSort` with other widely used implementations for 31-bit integers sorting. Note that the gap is larger for shorter keys. Most sorting implementations, like *Intel TBB parallel sort*, are comparison based sort which are not well suited for short integers. Intel `ippsSortRadixAscend_32s_I_L`, on the other hand, is well suited for integers but is not parallel, and it is not optimized for short keys. Our implementation is fully multi-threaded and takes advantage of the vectorization possibilities offered by modern computers such as the AVX512 extensions on the Xeon PHI. It has been developed primarily for sorting Hilbert indices, which are typically short. We use different strategies depending on the key bit size. This is the reason why `HXTSort` outperforms other sorting implementations when sorting Hilbert indices.

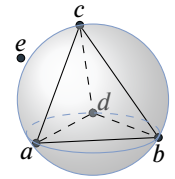
2.4 | Improving CAVITY: spending less time in geometric predicates

The first main operation of the Delaunay kernel is the construction of the cavity $C(DT_k, p_{k+1})$ formed by all the tetrahedra $\{a, b, c, d\}$ whose circumscribed sphere encloses p_{k+1} (Figure 1). This step of the incremental insertion represents about one third of the total execution time in available implementations (Table 1). The cavity is initiated with a first tetrahedron τ containing p_{k+1} determined with the WALK function (Algorithm 1 and Figure 1a), and then completed by inspection of neighboring tetrahedra with a breadth-first search algorithm.

Optimization of the `inSphere` predicate

A deeper look shows that the most expensive operation of the CAVITY function is the fundamental geometrical evaluation of whether a point e is inside/on/outside of the circumsphere of a tetrahedra $\{a, b, c, d\}$. To this end, the `inSphere` predicate computes the sign of the following determinant:

$$\text{inSphere}(a, b, c, d, e) = \begin{vmatrix} a_x & a_y & a_z & \|a\|^2 & 1 \\ b_x & b_y & b_z & \|b\|^2 & 1 \\ c_x & c_y & c_z & \|c\|^2 & 1 \\ d_x & d_y & d_z & \|d\|^2 & 1 \\ e_x & e_y & e_z & \|e\|^2 & 1 \end{vmatrix} = \begin{vmatrix} b_x - a_x & b_y - a_y & b_z - a_z & \|b - a\|^2 \\ c_x - a_x & c_y - a_y & c_z - a_z & \|c - a\|^2 \\ d_x - a_x & d_y - a_y & d_z - a_z & \|d - a\|^2 \\ e_x - a_x & e_y - a_y & e_z - a_z & \|e - a\|^2 \end{vmatrix}$$



This is a very time consuming computation, and to make it more efficient, we propose to expand the 4×4 determinant into a linear combination of four 3×3 determinants independent of point e .

$$\begin{aligned} \text{inSphere}(a, b, c, d, e) = & -(e_x - a_x) \begin{vmatrix} b_y - a_y & b_z - a_z & \|b - a\|^2 \\ c_y - a_y & c_z - a_z & \|c - a\|^2 \\ d_y - a_y & d_z - a_z & \|d - a\|^2 \end{vmatrix} + (e_y - a_y) \begin{vmatrix} b_x - a_x & b_z - a_z & \|b - a\|^2 \\ c_x - a_x & c_z - a_z & \|c - a\|^2 \\ d_x - a_x & d_z - a_z & \|d - a\|^2 \end{vmatrix} \\ & -(e_z - a_z) \begin{vmatrix} b_x - a_x & b_y - a_y & \|b - a\|^2 \\ c_x - a_x & c_y - a_y & \|c - a\|^2 \\ d_x - a_x & d_y - a_y & \|d - a\|^2 \end{vmatrix} + \|e - a\|^2 \begin{vmatrix} b_x - a_x & b_y - a_y & b_z - a_z \\ c_x - a_x & c_y - a_y & c_z - a_z \\ d_x - a_x & d_y - a_y & d_z - a_z \end{vmatrix} \end{aligned}$$

Being completely determined by the tetrahedron vertex coordinates, the four 3×3 determinants can be pre-computed and stored in the tetrahedron data structure when it is created. The cost of the `inSphere` predicate becomes then negligible. Notice also that the fourth sub-determinant is minus the tetrahedron volume. We can set it to a positive value to flag deleted tetrahedra during the breadth-first search, and save this way some memory space.

The maximal improvement of the CAVITY function obtained with this optimization depends on the number of times the `inSphere` predicate is invoked per tetrahedron. First, it is known that, in the final mesh, the number of tetrahedra is about 6 times the number of vertices²⁹. This means that each point insertion results in average in the creation of 6 new tetrahedra. On the other hand, we have seen in Section 2.3 that an appropriate point ordering ensures an approximately constant number of tetrahedra in the cavities. This number is close to 20 in a usual mesh generation context¹⁰. One point insertion results thus in the deletion of 20 tetrahedra, and the creation of 26 tetrahedra (all figures are approximations). This number is also the number of triangular faces of the cavity, since all tetrahedra created by the `DELAUNAYBALL` function associate a cavity face and the inserted vertex p_{k+1} . The number of evaluations of the `inSphere` predicate can thus now be evaluated quantitatively. It is evaluated (positively) for the 20 tetrahedra forming the cavity and (negatively) for the 26 tetrahedra adjacent to the faces of the cavity, so 46 times in total for each vertex insertion.

When n points have been inserted in the mesh, a total of $26n$ tetrahedra were created and the predicate has been evaluated $46n$ times. Thus, we may conclude from this analysis that the `inSphere` predicate is called approximately $46n/26n = 1.77$ times per tetrahedron. In consequence, the maximal improvement that can be obtain from our optimization of the `inSphere` predicate is of $1 - 1/1.77 = 43\%$. This has a cost in terms of memory (the storage of 4 `double` values per tetrahedron) and bandwidth (the loading and storing of sub-determinants). In our opinion, this speedup is worth the cost. For instance, for $n = 4 \cdot 10^6$, we observe a speedup of 32% in the `inSphere` predicate evaluations, taking into account the time spent to compute the stored sub-determinants.

A second geometric predicate is extensively used in Delaunay triangulation. The `orient3d` predicate evaluates whether a point d is above/on/under the plane defined by three points $\{a, b, c\} \in \mathbb{R}^3$ ³⁰. It computes the triple product $(b-a) \cdot ((c-a) \times (d-a))$, i.e. the signed volume of tetrahedron $\{a, b, c, d\}$. This predicate is mostly used in the `WALK` function.

Implementation details

Geometrical predicates evaluated with standard floating point arithmetics may lead to inaccurate or inconsistent results. To have a robust and efficient implementations of the `inSphere` and `orient3d` predicates, we have applied the strategy implemented in `Tetgen`².

1. Evaluate first the predicate with floating point precision. This gives a correct value in the vast majority of the cases, and represent only 1% of the code.
2. Use a filter to check whether the obtained result is certain. A simple static filter is used. If the standard formula is untrustworthy, the predicate is evaluated with exact arithmetics³⁰.
3. To be uniquely defined, Delaunay triangulations requires each point to be inside/outside a sphere, under/above a plane. When a point is exactly on a sphere or a plane, the point is in a non-general position and its position must be slightly perturbed to “escape” from this singularity. We have implemented the symbolic perturbations proposed by Edelsbrunner³¹.

We explain the slightly better efficiency of our implementation (Table 1) by data structure differences (Section 2.2).

2.5 | Improving DELAUNAYBALL: spending less time computing adjacencies

The `DELAUNAYBALL` function creates the tetrahedra filling the cavity (Figure 1c), and updates the mesh structure. In particular, tetrahedron adjacencies are recomputed. This is the most expensive step of the Delaunay triangulation algorithm as it typically takes about 40% of the total time (Table 1).

In contrast to existing implementations, we strongly interconnect the cavity building and cavity retriangulation steps. Instead of relying on a set of elegant and independent elementary operations like tetrahedron creation/deletion or adjacency computation, a specific cavity data structure has been developed, which optimizes batches of operations for the specific requirements of the Delaunay triangulation (Listing 2).

Use cavity building information The tetrahedra reached by the breadth-first search during the CAVITY step (Section 2.4), are either inside or adjacent to the cavity. Each triangular facet of the cavity boundary is thus shared by a tetrahedron $t_1 \in \mathcal{A}(\text{DT}_k, p_{k+1})$ outside the cavity, by a tetrahedron $t_2 \in \mathcal{C}(\text{DT}_k, p_{k+1})$ inside the cavity, and by a newly created tetrahedron inside the cavity $t_3 \in \mathcal{B}(\text{DT}_k, p_{k+1})$ (Figure 1). The facet of t_1 adjacent to the surface of the cavity defines, along with the point p_{k+1} , the tetrahedron t_3 . We thus a priori know that t_3 is adjacent to t_1 , and store this information in the `cavityBoundaryFacet_t` structure (Listing 2).

```

typedef struct {
    uint32_t new_tetrahedron_vertices[4]; // facet vertices + vertex to insert
    uint64_t adjacent_tetrahedron_ID;
} cavityBoundaryFacet_t
5
typedef struct{
    uint64_t adjacency_map[1024]; // optimization purposes, see Section 2.5

    struct {
10        cavityBoundaryFacet_t* boundary_facets;
        uint64_t num; // number of boundary facets
        uint64_t allocated_num; // capacity [in cavityBoundaryFacet_t]
    } to_create;

    struct {
15        uint64_t* tetrahedra_ID;
        uint64_t num; // number of deleted tetrahedra
        uint64_t allocated_num; // capacity [in uint64_t]
    } deleted;
20 } Cavity_t;

```

Listing 2: Cavity specific data structure

Fast adjacencies between new tetrahedra A bunch of information has been collected along the way when building the cavity: the list of involved vertices as well as all adjacencies with tetrahedra outside the cavity. It remains now to compute adjacencies between the tetrahedra in the cavity, i.e., the tetrahedra of the Delaunay ball.

The first vertex of all created tetrahedra is set to be p_{k+1} , whereas the other three vertices $\{p_1, p_2, p_3\}$ are on the cavity boundary, and are ordered so that the volume of the tetrahedral element is positive, i.e., $\text{orient3d}(p_{k+1}, p_1, p_2, p_3) > 0$. As explained in the previous section, the adjacency index $4t_i + 0$ corresponding to the face opposite to the vertex p_{k+1} is already known for all tetrahedra t_i in $\mathcal{B}(\text{DT}_k, p_{k+1})$. Three neighbors are thus still to be determined for each tetrahedron t_i , which means practically that an adjacency index has to be attributed to $4t_i + 1$, $4t_i + 2$ and $4t_i + 3$. The internal facets across which these adjacencies have to be identified are made of the common vertex p_{k+1} and one oriented edge of the cavity boundary.

Using an elaborated hash table with complex collision handling would be overkill for this identification task. We rather use a double entry lookup table of dimension $n \times n$, whose rows and columns are associated with the n vertices $\{p_j\}$ of the cavity boundary, to which auxiliary indices $0 \leq i_j < n$ are affected for convenience and stored in the padding variable of the vertex. With this, the unique index of an oriented edge $p_1 p_2$ is set to be $n \times i_1 + i_2$, which corresponds to one position in the $n \times n$ lookup table. So, for each tetrahedron t_i in the Delaunay ball with vertices $\{p_{k+1}, p_1, p_2, p_3\}$, the adjacency index $4t_i + 1$ is stored at position $n * i_2 + I_3$ in the lookup table, and similarly $4t_i + 2$ at position $n * i_3 + i_1$ and $4t_i + 3$ at position $n * i_1 + i_2$. A square array with a zero diagonal is built proceeding this way, in which the sought adjacencies are the pairs of symmetric components.

There is no maximal value for the number n of vertices in the cavity but, in practice, we can take advantage of the fact that it remains relatively small. The cavity boundary is the triangulation of a topological sphere. This is a planar graph for which it can be shown that the number of edges is $E = 3F/2$ edges, with F the number of faces, and that the Euler characteristic is $n - E + F = 2$. Hence, the number of vertices is related to the number of triangular faces by the relationship $n = F/2 + 2$. As we have shown earlier that F is about 26, we end up with an approximation of $n = 15$ vertices on a cavity boundary. Hence, a $n_{max} \times n_{max}$ lookup table, with maximum size $n_{max} = 32$ is sufficient provided there are at most $F_{max} = 2(n_{max} - 2) = 60$ tetrahedra created in the cavity, which is much more than the average number 26. If the cavity exceptionally contains more elements, the algorithm smoothly switches to a simple linear search.

Once all adjacencies of the new tetrahedra have been properly identified, the `DELAUNAYBALL` function is then in charge of updating the mesh data structure. This ends the insertion of point p_{k+1} . The space freed by deleted tetrahedra is reused, if needed additional tetrahedra are added. Note that almost all steps of adjacencies recovery are vectorizable.

2.6 | About a ghost

The Bowyer–Watson algorithm for Delaunay triangulation assumes all newly inserted vertex are inside an element of the triangulation at the previous step (Algorithm 1). To insert a point p_{k+1} outside the current support of the triangulation, one possible strategy is to enclose the input vertices in a sufficiently large bounding box, and to remove the tetrahedra lying outside the convex hull of the point set at the end of the algorithm. A more efficient strategy, adopted in TetGen², CGAL³, Geogram⁴, is however

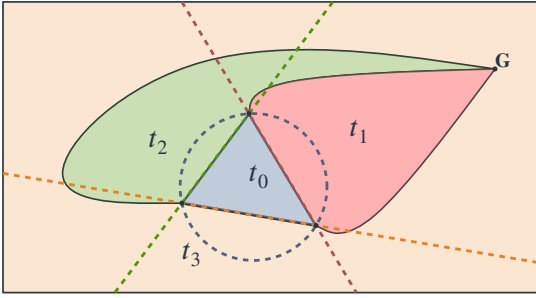


FIGURE 4 Triangle t_0 surrounded by three ghost triangles t_1 , t_2 and t_3 . Circumcircles are shown in dash lines of the respective color

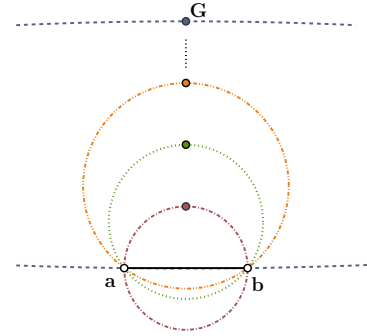


FIGURE 5 Circumcircles of an edge \overline{ab} and increasingly distant vertices. For a vertex G infinitely far away, the degenerate circle approaches a line.

to work with the so-called ghost tetrahedra connecting the exterior faces of the triangulation with a virtual ghost vertex G . With this elegant concept, vertices can be inserted outside the current triangulation support with almost no algorithmic change.

The ghost vertex G is the vertex "at infinity" shared by all ghost tetrahedra (Figure 4). The ghost tetrahedra cover the whole space outside the triangulation. Like regular tetrahedra, ghost tetrahedra are stored in the mesh data structure, and they get deleted whenever a vertex is inserted inside their circumsphere. The accurate definition of the circumsphere of a ghost tetrahedra, on particular with respect to the requirements of the Delaunay condition, is however a delicate question.

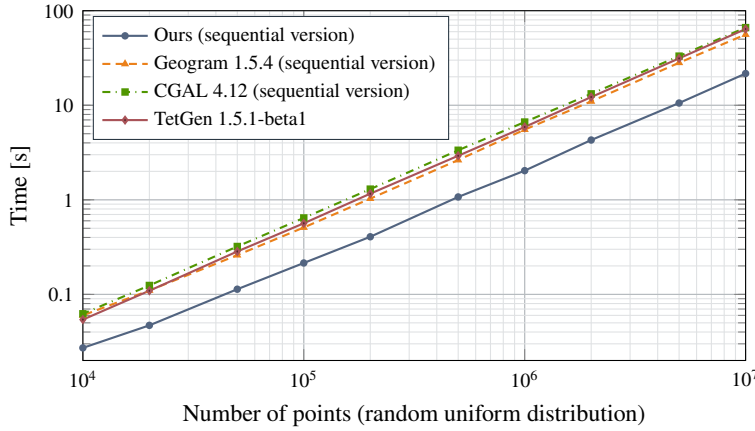
From a geometrical point of view, as the ghost vertex G moves away towards infinity from an exterior face abc of the triangulation, the circumscribed sphere of tetrahedron $abcG$ tends to the half space on the positive side of the plane determined by the points abc , i.e., the set of points x such that $\text{orient3d}(a, b, c, x)$ is positive. The delicate question is whether this inequality should be strict or not, and the robust answer is neither one nor the other.

This is illustrated in 2D in Figure 5. The circumcircle of a ghost triangle abG actually contains not only the open half-plane strictly above the line \overleftrightarrow{ab} , but also the line segment $[ab]$; the other parts of the line \overleftrightarrow{ab} being excluded. The additional component $[ab]$ is geometrically characterized as the part of the line ab that lies inside the circumscribed circle of the regular triangle adjacent to the face $[ab]$. In 3D, the circumsphere of a ghost tetrahedron $abcG$ contains the half-space L such that for any point $d \in L$, $\text{orient3d}(a, b, c, d)$ is strictly positive, plus the disk defined by the circumcircle of the face abc . If the point d is in the plane abc , i.e. $\text{orient3d}(a, b, c, d)=0$, we thus additionally test if d is in the circumsphere of the adjacent regular tetrahedron sharing the facet abc . This composite definition of the circumscribed circle is what makes the ghost tetrahedron technique robust with minimal algorithmic changes. In the implementation, this modification affects actually exclusively the `inSphere` predicate.

Because the 3×3 determinant of `orient3d` is used instead of the 4×4 determinant of `inSphere` for ghost tetrahedra, the approach with a ghost vertex is faster than other strategies¹³. Note that the `WALK` cannot evaluate `orient3d` on the faces of ghost tetrahedra that connect edges of the convex hull to the ghost vertex. If the starting tetrahedron is a ghost tetrahedron, the `WALK` directly steps into the non-ghost adjacent tetrahedron. Then, if it steps in a ghost tetrahedron $abcG$ while walking toward p_{k+1} , we have $\text{orient3d}(a, b, c, p_{k+1}) > 0$ and the ghost tetrahedron is inside of the cavity. The walk hence stops there, and the algorithm proceeds as usual.

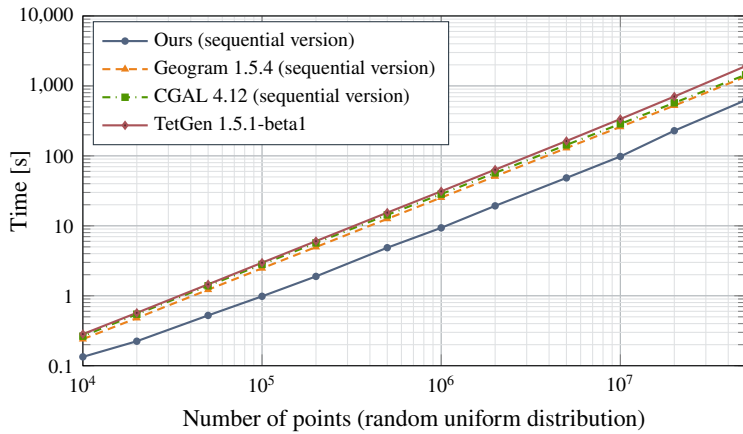
2.7 | Serial implementation performances

The code for the serial Delaunay triangulation has about one thousand lines (without Shewchuk's geometric predicates³⁰). Our implementation is open-source and available in Gmsh (www.gmsh.info). Overall, it is three time faster than other sequential implementations. Figure 6a and 6b show the performance gap between our implementation and concurrent software on a laptop with a maximum core frequency of 3.5Ghz, and on a many-core computer with a maximum core frequency of 1.5Ghz. Table 1 indicates that the main difference in speed comes from the more efficient adjacencies computation in the `DelaunayBall` function. Other software use a more general function that can also handle cavities with multiple interior vertices. But this situation does not happen with Delaunay insertion, where there is always one unique point in the cavity, p_{k+1} . Since our



# vertices	10^4	10^5	10^6	10^7
Ours	0.027	0.21	2.03	21.66
Geogram	0.060	0.51	5.53	56.02
CGAL	0.062	0.64	6.65	66.24
TetGen	0.054	0.56	5.89	63.99

(a) Intel® Core™ i7-6700HQ CPU, maximum core frequency of 3.5Ghz



# vertices	10^4	10^5	10^6	10^7
Ours	0.134	0.98	9.36	97.97
Geogram	0.240	2.47	25.34	259.74
CGAL	0.265	2.81	28.36	286.54
TetGen	0.283	2.97	31.13	336.21

(b) Intel® Xeon Phi™ 7210 CPU, maximum core frequency of 1.5Ghz

FIGURE 6 Performances of our sequential implementation of the Delaunay incremental point insertion (Algorithm 1) and comparison with CGAL, Geogram, and TetGen on a laptop (a) and on CPU with slow cores having AVX-512 vectorized instructions (b). Timings are in seconds and exclude the initial spatial sort.

`DelaunayBall` function is optimized for Delaunay cavities, it is approximately three time faster, despite the additional computation of sub-determinants. The remaining performance gain is explained by our choice of simple but efficient memory aligned data structure.

3 | PARALLEL DELAUNAY

3.1 | Related work

To overcome memory and time limitations of sequential Delaunay triangulation, a number of parallel algorithms have been proposed over the last two decades⁶. Most approaches partition the given point set into sub-domains, and apply to them an existing sequential meshing^{7,8}. The boundaries separating these sub-domains are first meshed in order to ensure mesh conformity across sub-domains interfaces, and the mesh of those surface boundaries act then as hard constraints for the sequential meshing procedure applied in each sub-domain. Such a “coarse grain” parallelization procedure has two main advantages: (i) using multiple computers means access to a larger memory space, necessary for the generation of very large meshes, (ii) the sequential

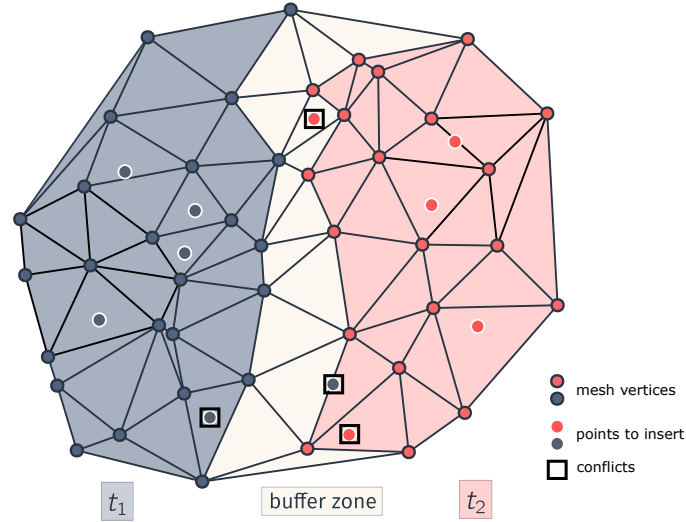


FIGURE 7 Vertices are partitioned such that each vertex belongs to a single thread. A triangle can only be modified by a thread that owns all of its three vertices. Triangles that cannot be modified by any thread form a buffer zone.

algorithms can be used with few modifications or even as is, e.g., the Pampa suite. Although impressive speedups may be obtained this way, coarse grain parallelization schemes do not tackle at all the issue of efficiency of the inherently sequential meshing. Moreover, the overheads of domain partitioning strategies are high and scaling is usually very limited.

The real challenge is to parallelize the Delaunay incremental insertion algorithm (Algorithm 1) at a fine grain level, i.e., to be able to concurrently insert points in a current Delaunay triangulation. To insert a point in a Delaunay triangulation, the kernel procedure operates on a cavity whose triangulation is modified to accommodate the inserted point (Figure 1). Two points can therefore be inserted concurrently in a Delaunay triangulation if their respective cavities do not intersect, $C(DT_k, p_{k1}) \cap C(DT_k, p_{k2}) = \emptyset$, otherwise there is a conflict. In practice, other types of conflicts and data-races should be taken into account, which depend tightly on the chosen data structures and the insertion point strategy. Conflict management strategies relying heavily on locks⁴ lead to relatively good speedups on small numbers of cores, e.g., a speedup of 5 on 8 cores⁹. In particular, our team has worked recently on a two-level approach¹⁰ allowing a speedup of 18 on 32 cores. Yet, synchronization overheads prevent those approaches to scale on larger numbers of cores.

3.2 | A parallel strategy based on partitions

There are multiple conditions a program should ensure to avoid data-races and conflicts between threads when concurrently inserting points in a Delaunay triangulation. Consider thread t_1 is inserting point p_{k1} and thread t_2 is simultaneously inserting point p_{k2} .

1. Thread t_1 cannot access information about any tetrahedron in $C(DT, p_{k2})$. Hence:

- (a) $C(DT, p_{k1}) \cap C(DT, p_{k2}) = \emptyset$
- (b) $\mathcal{A}(DT, p_{k1}) \cap C(DT, p_{k2}) = \emptyset$ and $\mathcal{A}(DT, p_{k2}) \cap C(DT, p_{k1}) = \emptyset$
- (c) Thread t_1 cannot walk into $C(DT, p_{k2})$ and reciprocally, t_2 cannot walk into $C(DT, p_{k1})$

2. A tetrahedron in $\mathcal{B}(DT, p_{k1})$ and a tetrahedron in $\mathcal{B}(DT, p_{k2})$ cannot be created at the same memory index.

To ensure rule (1) it is sufficient to restrain each thread to work on an independent partition of the mesh (Figure 7). This lock-free strategy minimize synchronization between threads and is very efficient. Each point of the Delaunay triangulation is assigned a partition corresponding to a unique thread. A tetrahedron belongs to a thread if at least three of its vertices are in that thread's partition.

³<https://project.inria.fr/pampa/>

⁴A lock is a synchronization mechanism enforcing that multiple threads do not access a resource at the same time. When a thread cannot acquire a lock, it usually waits.

To ensure (1a) and (1b), the insertion of a point belonging to thread aborts if it accessed a tetrahedron that belongs to another thread, or that is in the buffer zone. To ensure (1c), we forbid threads to walk in tetrahedra belonging to another thread. Consequently, a thread aborts the insertion of a vertex when (i) the WALK reaches another partition, or when (ii) the CAVITY function reaches a tetrahedron in the buffer zone. To insert these points, the vertices are re-partitioned differently (Section 3.3), a procedure repeated until there is no more vertices to insert or until the rate of successful insertions has become too low. In that case, the number of threads is lowered (Section 3.4). When the number of points to insert has become small enough, the insertion runs in sequential mode to insert all remaining vertices. The first BRIO round is always inserted sequentially to generate a first base mesh.

Rule (2) is obvious from a parallel memory management point of view. However, it is difficult to ensure it without requiring an unreasonable amount of memory. As explained in Section 3.6, at this step, synchronization between threads is required punctually.

3.3 | Partitioning and re-partitioning with Moore curve

We subdivide the n_v points to insert such that each thread inserts the same number of points. Our partitioning method is based on the Moore curve, i.e. on the point insertion order implemented for the sequential Delaunay triangulation (Section 2.3). Space-filling curves have already been used successfully for partitioning meshes^{32,33,34,35}. Each partition of the n_{thread} partitions is a set of grid cells that are consecutive along the Moore curve. To compute the partitions, i.e. its starting and ending Moore indices, we sort the points to insert according to their Moore indices (see Section 2.3). Then, we assign the first $n_v/n_{threads}$ points to the first partition, the next $n_v/n_{threads}$ to the second, etc (Figure 8c). The second step is to partition the current Delaunay triangulation in which the points are going to be inserted. We use again the Moore indices to assign the mesh vertices to the different partitions. The ghost vertex is assigned a random index. The partition owning a tetrahedron is determined from the partitions of its vertices, if it has at least three vertices in a partition it belong to this partition, otherwise the tetrahedron is in the buffer zone. Each thread then owns a subset of the points to insert and a subset of the current triangulations.

Once all threads attempted to insert all their points, a majority of vertices is usually correctly inserted. To insert the remaining vertices, for which insertion failed (Figure 7) because the point cavity spans multiple partitions, we modify the partitions. To modify significantly the partitions we modify the computation of the Moore indices by applying a coordinate transformation and a circular shift, so that the zero index is moved around the looping Moore curve (Figure 8). Coordinates below a random threshold are linearly compressed, while coordinates above the threshold are linearly expanded. Thanks to our partitioning strategy, the synchronization overhead is minimal.

3.4 | Ensuring termination

When the number of vertices of the current Delaunay triangulation is small, typically at the first steps of the algorithm, the probability that the mesh vertices belong to different partitions is very high and none of the point insertion may succeed. To avoid wasting precious milliseconds, the first BRIO round is always inserted sequentially.

Moreover, there is no guarantee that re-partitioning will be sufficient to insert all the points. And even when a large mesh is already constructed, parallel insertion could enter an infinite failure loop. After a few rounds, the remaining points to insert are typically located in very small areas (intersection of previous buffer zones). Because re-partitioning is done on the not-yet-inserted points, the resulting partitions will also be small and thin. This leads to inevitable conflicts as partitions get smaller than cavities. In practice, we observed that the ratio ρ of successful insertions decreases at a constant number of threads. If 80 out of 100 vertices are successfully inserted in a mesh ($\rho_k = 0.8$), less that 16 of the 20 remaining vertices will be inserted at the following attempt ($\rho_{k+1} < 0.8$). Note that this effect is more important for small meshes, because the bigger the mesh, the relatively smaller the buffer zone and the higher the insertion success rate. This difference explains the growth of the number of tetrahedra created per second with the number of points in the triangulation (Figure 10).

To avoid losing a significant amount of time in re-partitioning and trying to insert the same vertices multiple times we gradually decrease the number of threads. Choosing the adequate number of threads is a question of balance between the potential parallelization gain and the partitioning cost that comes with each insertion attempt. When decreasing the number of threads, we decrease the number of attempts needed. When the ratio of successful insertions is too low, $\rho < 1/5$, or when the number of points to insert per thread is under 3,000, we divide the number of threads by two. Furthermore, if $\rho_k \leq 1/n_{threads}$, the next insertion attempt will not benefit from multi-threading and we insert the points sequentially.

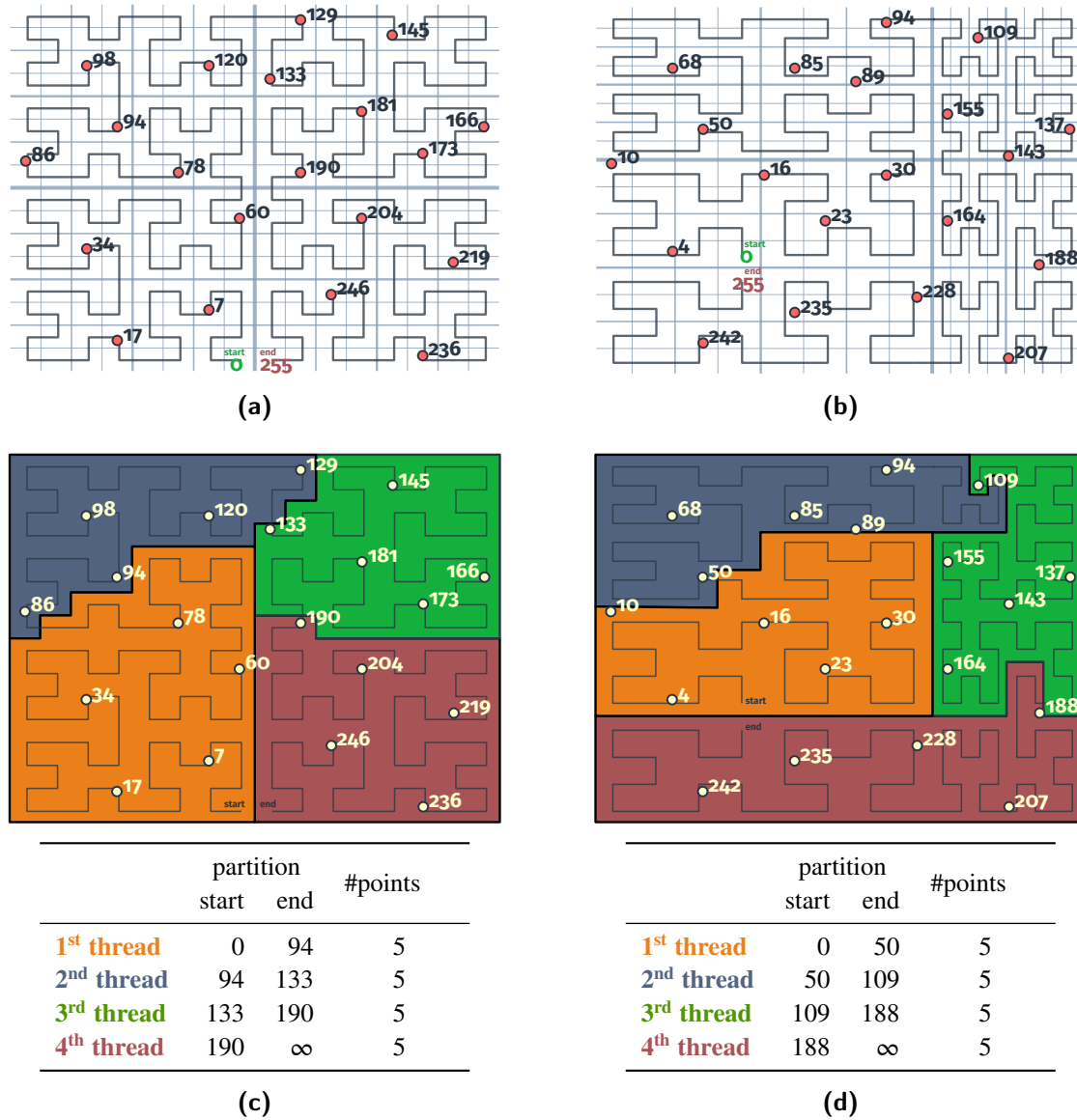


FIGURE 8 Partitioning of 20 points in 2D using the Moore indices, on the right the supporting grid of the Moore curve is transformed and the curve is shifted. In both cases, each partition contains 5 points. Indeed, the starting and ending Moore index of each partition are defined in a way that balances the point insertions between threads.

On Table 2 are given the number of threads used at each step of the Delaunay triangulation of a million vertices depending on the number of points to insert, the size of the current mesh, and the success insertion ratio ρ . Note that the computation of Moore indices and the sorting of vertices to insert are always computed on the maximal number of threads available (8 threads in this case) even when the insertion runs sequentially.

3.5 | Data structures

The data structure is similar to the one used by our sequential implementation (Section 2.2). There are two differences. First, the parallel implementation does not compute sub-determinants for each tetrahedron. Actually, the bandwidth usage with the parallel insertions is already near its maximum. Loading and storing sub-determinant becomes detrimental to the overall performance. Therefore, when running on a single core, our parallel implementation is a little bit slower than our sequential implementation. The four sub-determinants are replaced by a 16-bit color. A special color value flags deleted tetrahedra. Other possible color

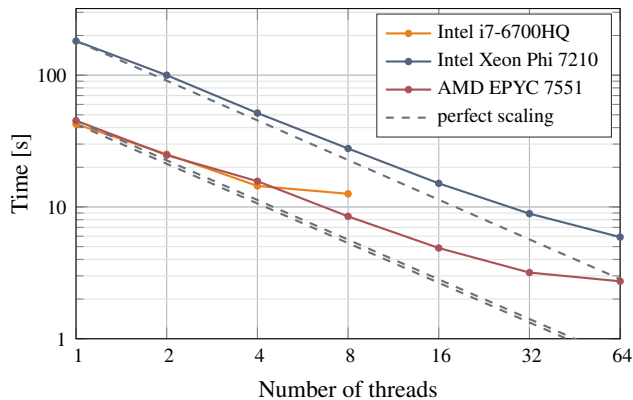


FIGURE 9 Scaling of our parallel Delaunay for a random uniform distribution of 15 million points, resulting in over 100 million tetrahedra on 3 machines: a quad-core laptop, an Intel Xeon Phi with 64 cores and a dual-socket AMD EPYC 2×32 cores.

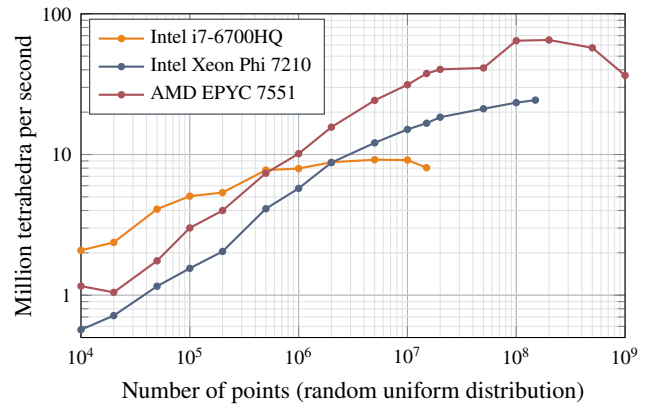


FIGURE 10 Number of tetrahedra created per second by our parallel implementation for different number of points. Tetrahedra are created more quickly when there is a lot of points because the proportion of conflicts is lower. A rate of 65 million tetrahedra created per second is obtained on the EPYC.

values distinguish different geometric entities. Second, each thread has its own `Cavity_t` structure (Listing 2) to which are added two integers identifying the starting and ending Moore indices of the thread's partition.

Memory footprint Because we do not store four sub-determinants per tetrahedra anymore but only a 2-bytes color, our mesh data structure is lighter. Still assuming that there is approximately $6n$ tetrahedra for n vertices, it requires a little more than $6 \times 50 + 32 = 332$ bytes per vertex. Thanks to this low memory footprint, we were able to compute the tetrahedrization of $N = 10^9$ vertices (about 6 billion of tetrahedra) on an AMD EPYC machine that has 512 GB of RAM.

3.6 | Critical operations

When creating new tetrahedra in the Delaunay ball of a point, a thread first recycle the space of its own array of deleted tetrahedra. When the `cavity->deleted.tetrahedra_ID` array of a thread is empty, additional memory should be allocated to this thread to create new tetrahedra. To limit allocation occurrences, each thread has an initial reserved space of 8,192 tetrahedra. When that space is used, 8,192 additional tetrahedra are reserved in the `cavity->deleted.tetrahedra_ID` thread array.

This operation is a critical part of the program requiring synchronization between threads to respect the rule (2). We need to capture the current number of tetrahedra and increment it by the number of tetrahedra in one single atomic operation. *OpenMP* provides the adequate mechanism, see Listing 3. Once the number of tetrahedra has been incremented atomically by at least 8,192, the thread fills the `cavity->deleted.tetrahedra_ID` with new indices of tetrahedra and flags them as deleted.

When the space used by tetrahedra exceeds the initially allocated capacity, reallocation is implemented that doubles the capacity of the array of mesh tetrahedra. During that operation, memory is potentially moved at another location. No other operation can be performed at that time on the mesh. Therefore, the reallocation code is placed in between two *OpenMP* barriers (Listing 4). This synchronization event is very rare and does not impact the performances. In general, a good estimation of the needed memory needed to reserve is possible and that critical section is never reached.

3.7 | Parallel implementation performances

We are able to compute the Delaunay of over one billion tetrahedra in record-breaking time: 41.6 seconds on the Intel Xeon Phi and 17.8 seconds on the AMD EPYC. This does not include I/O. As for the title of this article, we are able to generate three billion tetrahedra in 53 seconds on the EPYC. Performance comparisons with other implementations of parallel Delaunay are given on a laptop (Figure 11a) and on the Intel Xeon Phi (Figure 11b). The scaling of our implementation regarding the number of threads is detailed on Figure 9. Our code neither benefits from the 4-way hyperthreading of the Intel Xeon-Phi, nor from the

	#points		ρ	#threads	#mesh vertices
	to insert	success			
Initial mesh					4
BRIO Round 1	2044	2044	100%	1	2048
BRIO Round 2	12288	6988	57%	4	9036
	5300	3544	67%	2	12580
	1756	1756	100%	1	14336
BRIO Round 3	86016	59907	70%	8	74243
	26109	11738	45%	8	85981
	14371	7092	49%	4	93073
	7279	5332	73%	2	98405
	1947	1947	100%	1	100352
BRIO Round 4	602112	503730	84%	8	604082
	98382	44959	46%	8	649041
	53423	31702	59%	8	680743
	21721	7903	36%	8	688646
	13818	9400	68%	4	698046
	4418	3641	82%	2	701687
	777	777	100%	1	702464
BRIO Round 5	297536	271511	91%	8	973975
	26025	16426	63%	8	990401
	9599	8092	84%	4	998493
	1507	1507	100%	1	1000000

TABLE 2 Numbers of threads used to insert points in our parallel Delaunay triangulation implementation depending on the number of points to insert, the mesh size, the success rate of insertion at the previous step.

2-way simultaneous multithreading of the AMD EPYC. However, we obtain a good scaling until the number of threads reach the number of cores, i.e. 4 cores for the Intel i7-6700HQ, 64 cores for the Intel Xeon Phi 7210 and the AMD EPYC 7551. Our implementation clearly outperforms other existing implementations.

4 | TETRAHEDRAL MESH GENERATION

Algorithm 2 Mesh generation algorithm

Input: A set of triangles t

Output: A tetrahedral mesh \mathcal{T}

```

1: function PARALLEL MESHER( $t$ )
2:    $\mathcal{T}_0 \leftarrow \text{EMPTYMESH}(t)$ 
3:    $\mathcal{T} \leftarrow \text{RECOVERBOUNDARY}(\mathcal{T}_0)$ 
4:   while  $\mathcal{T}$  contains large tetrahedra do
5:      $S \leftarrow \text{SAMPLEPOINTS}(\mathcal{T})$ 
6:      $S \leftarrow \text{FILTERPOINTS}(S)$ 
7:      $\mathcal{T} \leftarrow \text{INSERTPOINTS}(\mathcal{T}, S)$ 
8:   end while
9:   return  $\mathcal{T}$ 
10: end function

```

```

if(cavity->to_create.num > cavity->deleted.num)
{
    uint64_t nTetNeeded = MAX(8192, cavity->to_create.num) - cavity->deleted.num;
5   uint64_t nTet;
    #pragma omp atomic capture
    {
        nTet = mesh->tetrahedra.num;
        mesh->tetrahedra.num+=nTetNeeded;
10    }

    reallocTetrahedraIfNeeded(mesh);
    reallocDeletedIfNeeded(state, cavity->deleted.num + nTetNeeded);

15    for (uint64_t i=0; i<nTetNeeded; i++){
        cavity->deleted.tetrahedra_ID[cavity->deleted.num+i] = 4*(nTet+i);
        mesh->tetrahedra.color[nTet+i] = DELETED_COLOR;
    }

20    cavity->deleted.num += nTetNeeded;
}

```

Listing 3: When there are less deleted tetrahedra than there are tetrahedra in the Delaunay ball, 8192 new "deleted tetrahedra" indices are reserved by the thread. As the mesh data structure is shared by all threads, `mesh->tetrahedra.num` must be increased in one single atomic operation.

```

void reallocTetrahedraIfNeeded(mesh_t* mesh)
{
    if(mesh->tetrahedra.num > mesh->tetrahedra.allocated_num)
    {
5       #pragma omp barrier

        // all threads are blocked except the one doing the reallocation
        #pragma omp single
        {
10         uint64_t nTet = mesh->tetrahedra.num;
            alignedRealloc(&mesh->tetrahedra.neighbor_ID, nTet*8*sizeof(uint64_t));
            alignedRealloc(&mesh->tetrahedra.vertex_ID, nTet*8*sizeof(uint32_t));
            alignedRealloc(&mesh->tetrahedra.color, nTet*2*sizeof(uint16_t));
            mesh->tetrahedra.allocated_num = 2*nTet;

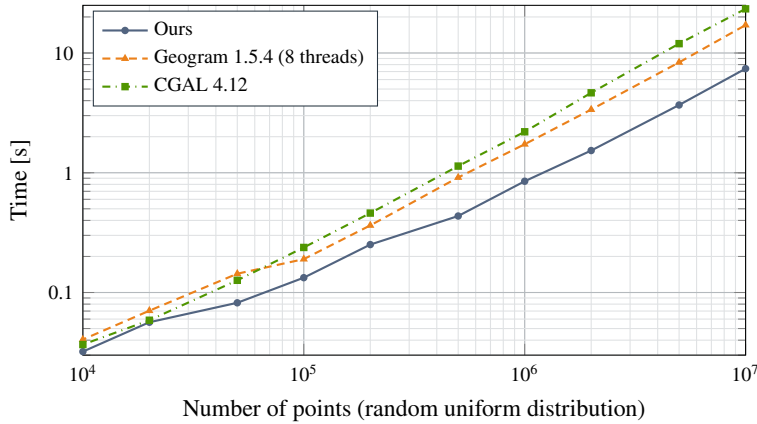
15         } // implicit OpenMP barrier here
    }
}

```

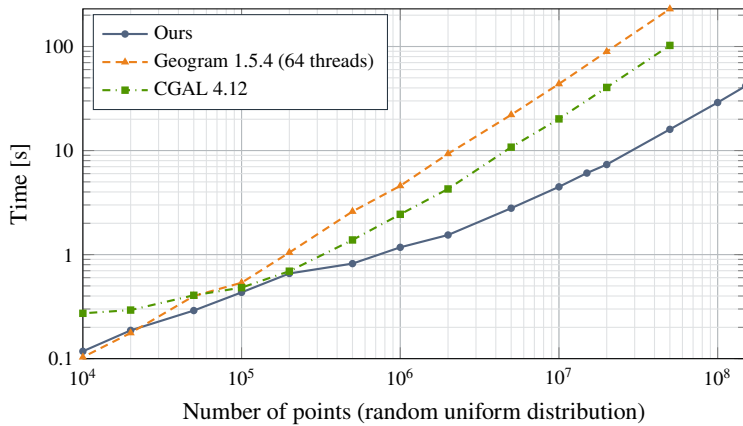
Listing 4: Memory allocation for new tetrahedra is synchronized with OpenMP barriers

The parallel Delaunay triangulation algorithm that we presented in the previous section is integrated in a Delaunay refinement mesh generator. A tetrahedral mesh generator is a procedure that takes as input the boundary of a domain to mesh, defined by set of triangles t that defines the boundary of a closed volume, and that returns a finite element mesh, i.e. a set of tetrahedra \mathcal{T} of controlled sizes and shapes which boundary is equal to the input triangulation: $\partial\mathcal{T} = t$. From a coarse mesh that is conformal to t , a Delaunay-refinement based mesher inserts progressively vertices until element sizes and shapes follow the prescribed ranges.

The mesh generation algorithm 2 proposed in this section follows the approach implemented for example in Tetgen². First, all the vertices of the boundary triangulation t are tetrahedralized to form the initial "empty mesh" \mathcal{T}_0 . Then, \mathcal{T}_0 is transformed into a conformal mesh \mathcal{T} which boundary $\partial\mathcal{T}$ is equal to t : $\partial\mathcal{T} = t$. The triangulation \mathcal{T} is then progressively refined by (i) creating vertices S at the circumcenters of tetrahedra which its circumspherere radius, r_r , is significantly larger that the desired mesh size, h , i.e. $r_r/h > 1.4$ ¹³ (ii) inserting the vertices in the mesh using our parallel Delaunay algorithm. The sets of points S to insert are filtered *a priori* in order not to generate short edges, i.e. edges of size smaller than $0.7h$. To avoid a costly filtering step, we use Hilbert coordinates to discard very close points on the curve, and implemented a slightly modified cavity algorithm (Section 2.4). Points are thus discarded both in the filtering process and in the insertion process. Note that contrary to existing implementations, we insert as large as possible point sets S during the refinement step to take advantage of the efficiency of our point insertion algorithm (Section 3). We parallelized all steps of the mesh generator (Algorithm 2) except the the boundary



(a) 4-core Intel® Core™ i7-6700HQ CPU.



(b) 64-core Intel® Xeon Phi™ 7210 CPU

FIGURE 11 Comparison of our parallel implementation with CGAL and Geogram on a high-end laptop (a) and a many-core computer (b). All timings are in seconds.

recovery procedure that is the one of Gmsh³⁶, which is essentially based on Tetgen². Note that we ensure that our final mesh is deterministic, i.e. and that for a given boundary surface mesh and prescribed size the output is reproducible.

Our mesh generator is at least one order of magnitude faster than state of the art meshers. We demonstrate its capabilities on various geometries and computers in the following of this section.

4.1 | Small and medium size test cases on standard laptops

In order to verify the scalability of the whole meshing process, meshes of up to one hundred million tetrahedra were computed on a 4 core 3.5 GHz Intel Core i7-6700HQ with 1, 2, 4 and 8 threads. Those meshes easily fit within the 8Gb of RAM of this modern laptop.

Three benchmarks are considered in this section: (i) a cube filled with cylindrical fibers of random radiuses and lengths that are randomly oriented, (ii) a mechanical part and (iii) a truck tire. Surface meshes are computed with Gmsh³⁶. Mesh size on the surfaces is controlled by surface curvatures and mesh size inside the domain is simply interpolated from the surface mesh.

Illustrations of the meshes, as well as timings statistics are presented in Figure 12. Performances of our code on a standard laptop are over one order of magnitude faster than state of the art meshers: our mesher is able to generate between 40 and 100 million tetrahedra per minute! Using multiple threads allows some speedup, the mesh refinement process is accelerated by a factor ranging between 2 and 3 on this 4 core machine.

The boundary recovery process is the bottleneck of our meshing process because it is not parallel yet. The last test case (truck tire) is defined by more than 7,000 CAD surfaces. Recovering the 27,892 triangular facets missing from \mathcal{T}_0 takes more than a third of the total meshing time with the maximal number of threads. Parallelizing the boundary recovery process is clearly a priority of our future developments. On this same example, the surface mesh was done with Gmsh using four threads. The surface mesher of Gmsh is not utterly fast and it took about the same time to generate the surface mesh of 6,881,921 triangles as to generate the volume mesh that contains over one hundred million tetrahedra using the same number of threads. The overall meshing time for the truck tire test case is thus about 6 minutes.

4.2 | Large mesh generation on many core machine

We further generated meshes containing over 300,000,000 elements on a AMD[®] EPYC 64 core machine. Three benchmarks are considered: (i) two cubes filled with many randomly oriented cylindrical fibers of random radiuses and lengths, and (ii) the exterior of an aircraft. Surface meshes were also generated by Gmsh.

Our strategy reaches its maximum efficiency for large meshes. In the 500 thin fibers test case, over 700,000,000 tetrahedra were generated in 135 seconds. This represents a rate of 5.2 million tetrahedra per second. In the 500 thin fibers test case, boundary recovery cost was lower and an impressive rate of 6,2 million tetrahedra per second was reached.

5 | CONCLUSION

This paper introduces a scalable Delaunay triangulation algorithm and demonstrates that inserting points concurrently can be performed effectively without the need of heavy synchronization mechanisms. We accelerate tetrahedral meshing procedures by one order of magnitude. This means that one of the goals of the HEXTREME ERC (European Research Council) Advanced Grant project awarded to Pr. Remacle is achieved. The key to our one order of magnitude faster algorithm is an optimization of the sequential and of the parallel algorithm highly specified for Delaunay meshing purposes. The lightweight Delaunay refinement based mesh generator presented in this paper is able to produce computational meshes with a rate above 5 million tetrahedra per second when state-of-the-art meshers typically produce about 5 million tetrahedra per minute. If minutes can become seconds, our methodology has the potential to become a game changer: such a speedup can definitively change the way engineers think about mesh generation.

When a procedure is parallelized, reproducibility is an issue. In the case of meshing, it is usually admitted that mesh generation should be deterministic for a given number of cores. Our meshing algorithm has been made deterministic in that sense, with a loss of 20% in overall performance. This feature has been implemented as an option. On the other hand, Figures 12 and 13 show that, starting from the same input, the number of elements varies when the number of cores varies. Making the code totally deterministic, i.e., designing an algorithm that would generate the same mesh independently of the number of cores would dramatically harm its scalability. This absence of absolute reproducibility is generally accepted in the engineering analysis community (note that the number of elements generally varies within a range that does not exceed 1%).

This paper is clearly not the end of the story. The first limitation that we will tackle is the parallelization of the boundary recovery procedure, which is crucial to generate meshes but also extremely costly in some cases. The next step is to include all other cavity operators in the same parallel framework in order to generate high-quality meshes: Edge swap, edge collapse, edge split, vertex relocation, face swap. Adaptive meshing will thus be the next outcome of this research. Then, the frontal point insertion strategy that has been proposed in³⁷ can also be parallelized using a similar strategy. Hex-dominant meshes will then be included in our new mesher, including boundary layer meshes.

ACKNOWLEDGMENTS

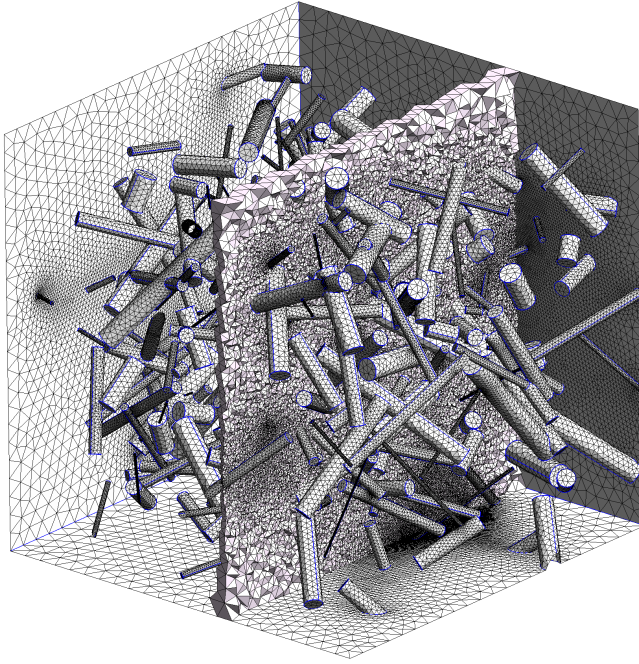
This research is supported by the European Research Council (project HEXTREME, ERC-2015-AdG-694020).

References

1. Cheng Siu-Wing. *Delaunay mesh generation*. Chapman & Hall/CRC computer and information science series Boca Raton: CRC Press; 2013.
2. Si Hang. TetGen, a Delaunay-Based Quality Tetrahedral Mesh Generator. *ACM Trans. Math. Softw.*. 2015;41(2):11:1–11:36.
3. Boissonnat Jean-Daniel, Devillers Olivier, Teillaud Monique, Yvinec Mariette. Triangulations in CGAL. In: :11–18ACM; 2000.
4. Levy B. *Geogram*. <http://alice.loria.fr/software/geogram/doc/html/index.html>; 2015.
5. Slotnick Jeffrey, Khodadoust Abdollah, Alonso Juan, et al. *CFD vision 2030 study: a path to revolutionary computational aerosciences*. : ; 2014. NASA.
6. Chrisochoides Nikos, Nave Damian. Parallel Delaunay mesh generation kernel. *International Journal for Numerical Methods in Engineering*. 2003;58(2):161–176.
7. Shostko Alexander, Löhner Rainald. Three-dimensional parallel unstructured grid generation. *International Journal for Numerical Methods in Engineering*. 1995;38(6):905–925.
8. De Cougny H. L., Shephard M. S.. Parallel refinement and coarsening of tetrahedral meshes. *International Journal for Numerical Methods in Engineering*. 1999;46(7):1101–1125.
9. Batista Vicente H.F., Millman David L., Pion Sylvain, Singler Johannes. Parallel geometric algorithms for multi-core computers. *Computational Geometry*. 2010;43(8):663–677.
10. Remacle Jean-François. A two-level multithreaded Delaunay kernel. *Computer-Aided Design*. 2017;85:2–9.
11. Frey Pascal Jean, George Paul-Louis. *Mesh Generation: Application to Finite Elements*. ISTE; 2007.
12. De Floriani Leila, Falcidieno Bianca, Nagy George, Pienovi Caterina. On sorting triangles in a delaunay tessellation. *Algorithmica*. 1991;6(1):522–532.
13. Shewchuk Jonathan R. *Delaunay refinement mesh generation*. : CARNEGIE-MELLON UNIV PITTSBURGH PA SCHOOL OF COMPUTER SCIENCE; 1997.
14. Boissonnat Jean-Daniel, Devillers Olivier, Hornus Samuel. Incremental Construction of the Delaunay Triangulation and the Delaunay Graph in Medium Dimension. In: SCG '09:208–216ACM; 2009; New York, NY, USA.
15. Amenta Nina, Choi Sunghee, Rote Günter. Incremental constructions con BRIO. In: Fortune Steven, ed. *Proceedings of the 19th ACM Symposium on Computational Geometry, San Diego, CA, USA, June 8-10, 2003*, :211–219ACM; 2003.
16. Haverkort Herman J., Walderveen Freek. Locality and bounding-box quality of two-dimensional space-filling curves. *Comput. Geom.*. 2010;43(2):131–147.
17. Abel David J., Mark David M.. A Comparative Analysis of some 2-Dimensional Orderings. *International Journal of Geographical Information Systems*. 1990;4(1):21–31.
18. Hamilton Chris H., Rau-Chaplin Andrew. Compact Hilbert indices: Space-filling curves for domains with unequal side lengths. *Inf. Process. Lett.*. 2008;105(5):155–163.
19. Blelloch Guy E.. Scans as Primitive Parallel Operations. *IEEE Trans. Computers*. 1989;38(11):1526–1538.
20. Zaghera Marco, Blelloch Guy E.. Radix sort for vector multiprocessors. In: Martin Joanne L., ed. *Proceedings Supercomputing '91, Albuquerque, NM, USA, November 18-22, 1991*, :712–721ACM; 1991.
21. Sohn Andrew, Kodama Yuetsu. Load balanced parallel radix sort. In: :305–312ACM; 1998.

22. Satish Nadathur, Harris Mark J., Garland Michael. Designing efficient sorting algorithms for manycore GPUs. In: :1–10IEEE; 2009.
23. Wassenberg Jan, Sanders Peter. Engineering a Multi-core Radix Sort. In: Jeannot Emmanuel, Namyst Raymond, Roman Jean, eds. *Euro-Par 2011 Parallel Processing*, :160–169Springer Berlin Heidelberg; 2011; Berlin, Heidelberg.
24. Polychroniou Orestis, Ross Kenneth A.. A comprehensive study of main-memory partitioning and its application to large-scale comparison- and radix-sort. In: Dyreson Curtis E., Li Feifei, Özsu M. Tamer, eds. *International Conference on Management of Data, SIGMOD 2014, Snowbird, UT, USA, June 22-27, 2014*, :755–766ACM; 2014.
25. Satish Nadathur, Kim Changkyu, Chhugani Jatin, et al. Fast sort on CPUs and GPUs: a case for bandwidth oblivious SIMD sort. In: Elmagarmid Ahmed K., Agrawal Divyakant, eds. *Proceedings of the ACM SIGMOD International Conference on Management of Data, SIGMOD 2010, Indianapolis, Indiana, USA, June 6-10, 2010*, :351–362ACM; 2010.
26. Merrill Duane, Grimshaw Andrew. High Performance and Scalable Radix Sorting: A case study of implementing dynamic parallelism for GPU computing. *Parallel Processing Letters*. 2011;21(02):245–272.
27. Bell Nathan, Hoberock Jared. Thrust: A productivity-oriented library for CUDA. In: Elsevier 2011 (pp. 359–371).
28. Sengupta Shubhabrata, Harris Mark J., Zhang Yao, Owens John D.. Scan primitives for GPU computing. In: Segal Mark, Aila Timo, eds. *Proceedings of the ACM SIGGRAPH/EUROGRAPHICS Conference on Graphics Hardware 2007, San Diego, California, USA, August 4-5, 2007*, :97–106Eurographics Association; 2007.
29. Remacle Jean-François, Shephard Mark S. An algorithm oriented mesh database. *International Journal for Numerical Methods in Engineering*. 2003;58(2):349–374.
30. Shewchuk Jonathan Richard. Adaptive precision floating-point arithmetic and fast robust geometric predicates. *Discrete & Computational Geometry*. 1997;18(3):305–363.
31. Edelsbrunner Herbert, Mücke Ernst P.. Simulation of simplicity: a technique to cope with degenerate cases in geometric algorithms. *ACM Trans. Graph.*. 1990;9(1):66–104.
32. Lieber Matthias, Grützun Verena, Wolke Ralf, Müller Matthias S., Nagel Wolfgang E.. FD4: A Framework for Highly Scalable Load Balancing and Coupling of Multiphase Models. *AIP Conference Proceedings*. 2010;1281(1):1639-1642.
33. Aluru S., Sevilgen F. E.. Parallel domain decomposition and load balancing using space-filling curves. In: :230-235; 1997.
34. Devine Karen D, Boman Erik G, Heaphy Robert T, et al. New challenges in dynamic load balancing. *Applied Numerical Mathematics*. 2005;52(2-3):133–152.
35. Loseille Adrien, Menier Victorien, Alauzet Frédéric. Parallel Generation of Large-size Adapted Meshes. *Procedia Engineering*. 2015;124:57 - 69. 24th International Meshing Roundtable.
36. Geuzaine Christophe, Remacle Jean-François. Gmsh: A 3-D finite element mesh generator with built-in pre- and post-processing facilities. *International Journal for Numerical Methods in Engineering*. 2009;79(11):1309–1331.
37. Baudouin Tristan Carrier, Remacle Jean-François, Marchandise Emilie, Henrotte François, Geuzaine Christophe. A frontal approach to hex-dominant mesh generation. *Advanced Modeling and Simulation in Engineering Sciences*. 2014;1(1):1.





100 fibers

# threads	# tetrahedra	t_{brec}	t_{ref}	t
1	12,608,242	0.74	19.6	20.8
2	12,600,859	0.72	13.6	14.6
4	12,567,576	0.72	8.7	9.8
8	12,586,972	0.71	7.6	8.7

300 fibers

# threads	# tetrahedra	t_{brec}	t_{ref}	t
1	52,796,891	6.03	92.4	101.3
2	52,635,891	5.76	61.2	69.0
4	52,768,565	5.71	39.4	46.8
8	52,672,898	5.67	32.5	39.8



Mechanical part

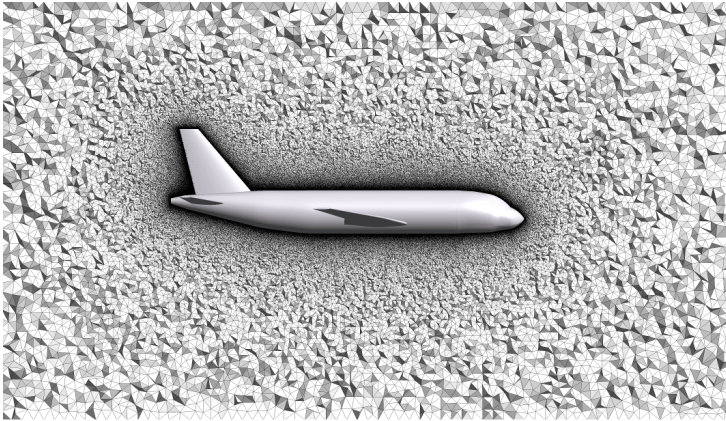
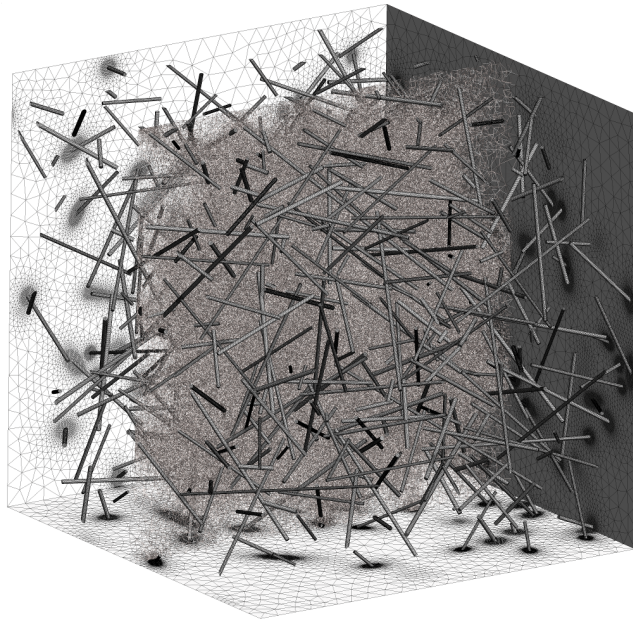
# threads	# tetrahedra	t_{brec}	t_{ref}	t
1	24,275,207	8.6	43.6	56.3
2	24,290,299	8.4	30.4	41.8
4	24,236,112	8.1	24.6	35.3
8	24,230,468	8.1	21.8	32.6



Truck tire

# threads	# tetrahedra	t_{brec}	t_{ref}	t
1	123,640,429	75.9	259.7	364.7
2	123,593,913	74.5	166.8	267.1
4	123,625,696	74.2	107.4	203.6
8	123,452,318	74.2	95.5	190.0

FIGURE 12 Performances of our mesh generator using a 4-core standard laptop: t_{brec} is the boundary recovery time, t_{ref} is the time for refining the mesh, and t is the wall clock time for the whole meshing process, including the generation of \mathcal{T}_0 and IOs.



100 thin fibers

# threads	# tetrahedra	t_{brec}	t_{ref}	t
1	325,611,841	3.1	492.1	497.2
2	325,786,170	2.9	329.7	334.3
4	325,691,796	2.8	229.5	233.9
8	325,211,989	2.7	154.6	158.7
16	324,897,471	2.8	96.8	100.9
32	325,221,244	2.7	71.7	75.8
64	324,701,883	2.8	55.8	60.1
127	324,190,447	2.9	47.6	52.0

500 thin fibers

# threads	# tetrahedra	t_{brec}	t_{ref}	t
1	723,208,595	18.9	1205.8	1234.4
2	723,098,577	16.0	780.3	804.8
4	722,664,991	86.6	567.1	659.8
8	722,329,174	15.8	349.1	370.1
16	723,093,143	15.6	216.2	236.5
32	722,013,476	15.6	149.7	169.8
64	721,572,235	15.9	119.7	140.4
127	721,591,846	15.9	114.2	135.2

Aircraft

# threads	# tetrahedra	t_{brec}	t_{ref}	t
1	672,209,630	45.2	1348.5	1418.3
2	671,432,038	42.1	1148.9	1211.5
8	665,826,109	39.6	714.8	774.8
64	664,587,093	38.7	322.3	380.9
127	663,921,974	38.1	255.0	313.3

FIGURE 13 Performances of our mesh generator using a AMD® EPYC® 64 core machine: t_{brec} is the boundary recovery time, t_{ref} is the time for refining the mesh, and t is the wall clock time for the whole meshing process, including the generation of \mathcal{T}_0 and IOs.